Journal of Materials Chemistry B

PAPER

Cite this: J. Mater. Chem. B, 2016, 4, 4771

# The effect of local delivery of adiponectin from biodegradable microsphere–scaffold composites on new bone formation in adiponectin knockout mice†

Dan Li,‡[ab] Yuan Guo,‡[ab] Hui Lu,‡[ab] Ren Wang,[ab] Hong-cheng Hu,[ab] Song-he Lu,[ab] Xue-fen Li,[b] Zi-chen Li,[c] Yu-wei Wu*[ab] and Zhi-hui Tang*[ab]

Received 19th March 2016,
Accepted 8th June 2016

DOI: 10.1039/c6tb00704j

www.rsc.org/MaterialsB

Adiponectin (APN) is the most abundant adipocyte-secreted adipokine; it regulates energy homeostasis and exerts well-characterized insulin-sensitizing properties. Previous studies have verified that globular adiponectin (gAPN) is also involved in bone metabolism, although observations have been controversial. The purpose of the current study is to use an APN-knockout (APN-KO) mouse model to evaluate the local delivery of gAPN to new bone formation. Using chitosan microspheres (CMs), we found that following an initial burst at 1 week, the release behavior of gAPN from the scaffold was sustained in a linear manner for the first 4 weeks, followed by a slower, more stable release from week 5 onwards. Interestingly, PLGA/β-TCP/CM-loaded gAPN scaffolds implanted in APN-KO mice increased bone formation and mineralization, and enhanced osteogenic marker expression 28 days post-implantation. gAPN also promoted preosteoblast (MC3T3-E1) cellular proliferation *in vitro*. In MC3T3-E1 cells, adaptor protein-containing pleckstrin homology domain, phosphotyrosine domain, leucine zipper motif (APPL1) and phosphoinositide 3-kinase (PI3K) expression was upregulated in a time-dependent manner upon gAPN treatment, while APPL1 small interfering RNA (siRNA) pre-treatment reversed this enhanced expression. In conclusion, modified bone graft substitutes loaded with gAPN increase bone formation and mineralization in part by promoting osteoblast proliferation *via* the APPL1/PI3K pathway.

## Introduction

Bone defects are one of the most commonly encountered problems in clinical practice. Existing bone defect treatment modalities include autogenous, allogenic, and synthetic bone grafts, with autografts as the preferred choice for bone grafting materials.[1,2] However, autografts require a second surgery and can cause morbidity, and the limited quantities of donor tissue and allografts lead to inherent problems of their own, such as possible transmission of donor pathogens, immunogenic response by the host, and high risk of infection.

On the other hand, many composite scaffolds have been successfully prepared by combining synthetic polymers or natural biopolymers with inorganic bioactive fillers such as poly(lactic-*co*-glycolic acid) (PLGA) chitosan microspheres (CMs) and β-tricalcium phosphate (β-TCP).[3–6] Biodegradable PLGA scaffolds combined with the controlled release of peptides and proteins by CMs are commonly used biomaterials for bone tissue engineering.[7,8] PLGA is well known for its excellent biocompatibility and controlled degradation rate. However, the PLGA scaffold surface is hydrophobic and lacks a cell-recognizing signal interface. The combination of PLGA with CMs and β-TCP may ameliorate these disadvantages. Chitosan has excellent biological properties with regard to biodegradability, biocompatibility, lack of toxicity, and bacteriostatic and adhesive properties, and is widely employed for the controlled delivery of peptides or proteins contained in microspheres.[9] CMs were introduced into the PLGA scaffolds to eliminate the need for organic solvents therein, which may cause structural damage to growth factor proteins, as well as to sustain delivery of the biologically active cytokines over an extended period of time. β-TCP was also embedded into the scaffold to increase the amount of cell-recognizing surface.[10,11] The incorporation of β-TCP led to a significant increase in water

[a] 2nd Dental Center, Peking University School and Hospital of Stomatology, B5 Anli Garden, #66 Anli Road, Chao Yang District, Beijing, 100101, China. E-mail: yuweiwu@bjmu.edu.cn, tang_zhihui@live.cn; Fax: +8610-64907970
[b] National Engineering Laboratory for Digital and Material Technology of Stomatology, Peking University School and Hospital of Stomatology, Beijing, China
[c] Department of Polymer Science & Engineering College of Chemistry & Molecular Engineering, Peking University, Beijing, China

† Electronic supplementary information (ESI) available. See DOI: 10.1039/c6tb00704j

‡ These authors equally contributed.

absorption by the scaffolds.[12] β-TCP is porous and entraps growth factors within its micropores, thereby prolonging their activity.[13] Fast degradation of β-TCP leads to the release of calcium ions, one of the main components of bone, facilitating the formation of new bone. In addition, β-TCP is well-known for its osteoinductive capabilities, triggering BMP expression upon direct contact with cells.[14,15] Proliferation of human osteogenous cells and synthesis of extracellular bone matrix are significantly enhanced in a dose-dependent manner with increasing doses of β-TCP;[15] furthermore, scaffolds constructed with β-TCP enhance the osteogenic differentiation of human bone marrow-derived mesenchymal stem cells (h-BMSCs), possibly *via* activation of the MAPK/ERK signaling pathway.[16,17] Nevertheless, PLGA-based implant systems can lead to severe inflammatory responses[18] which compromise healing[11] at the local implant site; in some cases additional surgery is required in order to re-implant the scaffold.[19] Bioactivity and osteogenesis of PLGA and β-TCP composites need to thereby be further enhanced to be of better use as implant materials in bone graft substitutes.

Due to the aforementioned limitations associated with PLGA composites, a combination of growth factors with engineered biomaterials has emerged as a new treatment alternative in bone repair and regeneration. Delivery of growth factors *via* optimally designed biodegradable scaffolds can stimulate cellular adhesion, proliferation, and differentiation, thus promoting bone regeneration.[4,13,15,19–21] Adiponectin (APN) present in plasma (20–30 μg $ml^{-1}$)[22,23] is the most abundant adipocyte-secreted adipokine,[24] and is comprised of trimers, hexamers, and high molecular weight multimers of full-length APN (fAPN).[25,26] The trimeric form of globular APN (gAPN), which results from proteolytic cleavage of fAPN, is also found in plasma.[27] APN displays well-characterized insulin-sensitizing, anti-inflammatory, anti-atherosclerotic, and anti-diabetic properties.[28,29] Ample clinical research data have demonstrated an association between APN and bone metabolism in various patient populations, however, with conflicting results.[30–32]

In this study, CMs loaded with APN were developed using emulsion-ionic cross-linking and then embedded into a PLGA/β-TCP scaffold to extend the APN release time. Consequently, we focused on exploring the long-term effects of gAPN on bone metabolism in APN knockout (APN-KO) mice. The aims of this study were twofold: (1) to elucidate the long term effects of controlled release of APN by a microsphere–scaffold complex carrier system on the induction of mineralized tissue formation in a male APN-KO mouse model, and (2) to explore possible molecular mechanisms underlying APN promotion of osteogenic effects in MC3T3-E1 cells.

## Materials and methods

### Recombinant gAPN

The pEt15b bacterial expression vector encoding the C-terminal domain of human APN (amino acids 106–244) was used to express gAPN with a histidine marker (His-gAPN) in BL21 (DE3) bacterial cells. His-gAPN was then purified using a GE Pharmacia AKTA Purifier 10 (Ramsey, MN, USA) followed by endotoxin removal using a ToxinEraser™ Endotoxin Removal Kit L00338 (GenScript, Piscataway, NJ, USA) and isolation using Zeba Spin Desalting Columns, 7k MWCO, 10 ml (Pierce, Rockford, IL, USA). The gAPN solution was passed through a 0.22 μm pore filter to remove bacteria.

### Materials

Chitosan (MW = 500 kDa, with a deacetylation grade of 90%), tripolyphosphate (TPP) and Span-80 were purchased from Beijing Chemical Reagents Company (Beijing, China). PLGA (nLA/nGA = 50/50) was obtained from Jinan Daigang Bioengineering Co. Ltd (Jinan, Shandong, China), and β-TCP was prepared in our lab. All other chemicals were of analytical grade and used as received in accordance with the manufacturer's instructions. All chemicals were sterilized with cobalt-60 gamma radiation prior to use.

### Preparation and characterization of scaffolds

CMs were formulated by emulsion-ionic cross-linking. Briefly, chitosan (900 mg) was dissolved in 2% (v/v) aqueous acetic acid (29 ml), and then 1 mg of gAPN in 1 ml of 2% (v/v) aqueous acetic acid was added. This mixture was poured into liquid paraffin (300 ml) containing 2% (v/v) of Span-80 and stirred mechanically for 2 h (C-MAG HS 10, IKA® Works Inc., Wilmington, NC, USA). Next, 5% (w/v) TPP (70 ml) was slowly added to the emulsion and stirred for 4 h at room temperature. The microspheres were isolated by repeated washings with excess amounts of petroleum ether, isopropyl alcohol, and distilled water prior to lyophilization. Microsphere–scaffold composites were fabricated *via* thermally induced phase separation. Next, 720 mg of PLGA was dissolved in 1,4-dioxane (12 ml), and after stirring for 30 min, 360 mg of β-TCP was added to the mixture.

An ultrasonic homogenizer (HuaNan Ultrasonic Equipment Co., Ltd Guangzhou, China) was used to disperse the β-TCP for 10 min. CMs loaded with APN (240 mg) were subsequently added to the solution. The solution was then stirred to completely disperse the microspheres. Afterwards, the mixture was immediately frozen with liquid nitrogen. Finally, PLGA/β-TCP/CM scaffolds with or without APN were acquired following overnight lyophilization at −20 °C according to the manufacturer's instructions (Labconco, Kansas City, MO, USA). Scaffolds without APN were used as an experimental control. The above procedures were conducted under aseptic conditions.

### Scanning electron microscopy (SEM)

The PLGA/β-TCP and CM surface structures were examined using a Hitachi S-4800 field-emission scanning electron microscope (Hitachi Ltd, Chiyoda, Tokyo, Japan) at an accelerating voltage of 20 kV. Samples were sputter coated with 50 nm gold particles under vacuum.

### *In vitro* hydrolytic degradation

PLGA/β-TCP/CM scaffolds with or without APN were prepared as cylinders with a diameter of 7 mm and a height of 5 mm. All samples were placed in 10 ml of PBS (0.1 M, pH 7.4) for

 

degradation. All experiments were performed in a shaking incubator at 37 °C at a speed of 100 rpm (Shanghai Hasuc Instrument Manufacture Co., Ltd, Shanghai, China). During the degradation process, the pH value of the degradation media was monitored using a pH meter (HANNA Instruments, Woonsocket, RI, USA) at predetermined time points. Three samples were prepared for each scaffold and reported pH values represent an average of the three samples.

### *In vitro* release study

The APN release study was carried out in PBS (pH 7.4, 0.05 mol $L^{-1}$) containing 0.01% sodium azide as a preservative. The microsphere–scaffold composite (about 20 mg) was placed in 10 ml of PBS at 37 °C at a rotation speed of 70 rpm. At predetermined time intervals, tubes were centrifuged at 2000 rpm for 5 min. The supernatant (1 ml) was removed, 1 ml of fresh solution was added, and APN concentration was measured using a Pierce™ Micro BCA™ Protein Assay kit (Thermo Scientific, Rockford, IL, USA). PLGA/CA without gAPN was used as a control. All of the data presented in this report are the mean data from 3 replicate samples.

### Animal experimentation and surgical procedures

Male APN-KO (Jax #008195) mice weighing 20–25 g were used. All protocols using mice were carried out under the guidelines described in the Association for Assessment and Accreditation of Laboratory Animal Care with approval (LA2013-4) from the Peking University Health Center Institutional Animal Care and Use Committee and Peking University Health Center Ethics Committee. All surgeries were performed by one person, and all efforts were made to minimize animal suffering and to reduce the number of animals used. Under general anesthesia (sodium pentobarbital 0.2 ml/100 g body weight, IP), mice were pronated, the skin over the thigh muscle was disinfected with iodine solution and ethanol, and then incised, exposing the hind limb fascia, followed by blunt dissection for muscle pouch formation. For the experimental group, gAPN-loaded scaffolds (3 × 3 × 3 mm) were implanted into the right and left thigh muscles of 4-week-old mice. In control mice, blank scaffolds were implanted following the same protocol. Mice in both groups then received calcein (10 mg $kg^{-1}$, Sigma-Aldrich, St. Louis, MO, USA) injections at 1 and 25 days post-implantation. Mice were sacrificed at 4 weeks post-implantation. Bone samples were isolated, fixed in 4% formalin solution overnight, and then scanned by micro-CT (μCT), dehydrated, and embedded in paraffin.

### μCT examination

Radiographs of bone samples were scanned using a high-resolution μCT system (Inveon, Siemens, Germany). Specimens were scanned at 60 kV, 300 μA, and 8.5 μm effective pixel size. Images were analyzed using software provided by the manufacturer. All images were captured using the following parameters: Ct = −550; $W$ = 550. Tissue bone mineral density (T-BMD) was then evaluated. T-BMD differs from bone mineral density (BMD) and can be used to estimate tissue mineral density (TMD).[33] TMD differs from bone mineral density (BMD) in that TMD is calculated from the average attenuation value of the bone tissue only and does not include attenuation values from non-bone voxels, as is done for BMD (whether volumetric or areal).

### Flow cytometry

To analyze immunogenic responses, blood was collected from the APN-loaded scaffold (experimental group) or the angular vein (control group) at 1 week post-implantation. The percentages of CD4+ and CD8+ T lymphocyte subpopulations and the ratios of CD4+/CD8+ T lymphocytes in peripheral blood from implant recipients were detected by flow cytometry.

Blood cells from the angular vein were dispersed into single-cell suspensions and stained with monoclonal antibodies (mAb) against human cell surface antigens, CD4 fluorescein isothiocyanate (FITC), CD8 phycoerythrin (PE), and CD3 peridinin chlorophyll protein (PerCP) (BD Biosciences, San Jose, CA, USA). For surface staining, cells were maintained in the dark at 4 °C throughout. Cells were washed twice in ice-cold FACS buffer (2% fetal calf serum, 0.1% $NaN_3$ in PBS), then incubated with each antibody and conjugate layer for 30 min and washed thoroughly with FACS buffer between layers. Flow cytometry analyses were performed on either a BD LSR II or BD FACSCanto II (BD Biosciences) and analyzed using FlowJo software (Tree Star, Ashland, OR, USA).

### Histological analysis and immunohistochemistry (IHC)

For histological analysis, samples were demineralized in 15% EDTA, dehydrated in graded alcohols and xylene, embedded in paraffin, and cut serially into 5 μm sagittal sections. The sections were then stained with hematoxylin–eosin (H&E). For IHC, the sections were deparaffinized and incubated with specific antibodies to detect expression of osteopontin (OPN). OPN (FL-314, 1 : 000) (sc-20788, Santa Cruz Biotechnology, CA, USA) is a rabbit polyclonal antibody which is used to detect OPN expression in humans, mice and rats. Anti-rabbit IgG (H+L) F(ab′)2 fragments (Cell Signalling Technology, MA, USA.) were conjugated to Alexa Fluor® 555 dye and detected using a LSM510 confocal scanning laser microscope (Zeiss, Germany).

### Quantitative real-time PCR

The composite transplantation region was dissected and homogenized. Total RNA was extracted using TRIzol (Invitrogen, Carlsbad, CA). Reverse transcription was performed using an iScript cDNA Synthesis Kit (Bio-Rad, Hercules, CA) in a 20 μl reaction volume containing 1 μg of total RNA, incubated at 25 °C for 5 min, transcripted at 42 °C for 30 min, and terminated by heating at 85 °C for 5 min. Real-time PCR was performed with Power SYBRGreen PCR Master Mix using a 7500 real-time PCR system (Applied Biosystems, Foster, CA). The reactions were run in duplicates with 1 μl of cDNA template in a 20 μl reaction volume with the program running at 50 °C for 2 min and 95 °C for 10 min, followed by 40 cycles at 94 °C for 15 s and 60 °C for 1 min. The amplification specificity was confirmed by the melting curve. The mRNA level of the target gene was acquired from the value of the threshold cycle (Ct) as a relative level to that of β-actin through the formula $2^{-\Delta Ct}$ (ΔCt = β-actin Ct – gene of interest Ct). The primers were

synthesized according to the previous study as follows: OPN sense/antisense, 5′-CTGCATACTGTAACCGCAGTC-3′/5′-CTCTC CATCCATAACATGGGC-3′;OCN sense/antisense, 5′-AGCCACCG AGACACCATGAGA-3′/5′-TAGCCACCGAGACACCATGAGA-3′; β-actin sense/antisense, 5′-TGA CAG GAT GCA GAA GGA GA-3′/5′-TAG AGC CAC CAA TCC ACA CA-3′.

### Cell proliferation analysis

The 25 mg PLGA/β-TCP/CMs loaded with APN were extracted in 5 ml of α-MEM supplemented with 10% FBS, 1% penicillin, and 100 μg $ml^{-1}$ of streptomycin sulfate for 7 days at 4 °C. Approximately $1 \times 10^3$ MC3T3-E1 cells per well were seeded in a 96-well plate and cultured to allow cell attachment. After incubation in 100 μl of extract (test groups) or α-MEM (control group) with 10% FBS, cell proliferation was measured at 12, 24, 48 and 72 h using a Cell Counting Kit-8 (CCK-8) assay. Next, 20 μl of CCK-8 solution was added to each well. The plates were incubated in a cell incubator for 1 h. Cell proliferation was analyzed using a microplate reader at a wavelength of 450 nm (BioTek, Winooski, VT, USA). Each experiment was performed in triplicate.

### APN treatment and siRNA-mediated knockdown of APPL1 in MC3T3-E1 cells

To further explore a possible signal transduction pathway for APN in promoting the proliferation of preosteoblasts, MC3T3-E1 cells were treated with gAPN or APPL1 siRNA. MC3T3-E1 cells were grown in α-MEM with 10% FBS in a 60 mm dish. Once the cells reached approximately 80% confluence, cells were cultured in α-MEM medium without FBS for 24 h followed by gAPN treatment for 15, 30, 60, and 120 min.

For APPL1 siRNA transfection, cells were grown in normal growth medium in a 6-well plate. When cells reached approximately 50% confluence, a pool of 3 target-specific 19–25 nucleotide small interfering RNA (siRNA) sequences (Santa Cruz Biotechnology Inc., Santa Cruz, CA, USA) either specifically designed to knockdown APPL1 or containing scrambled siRNA were tested in MC3T3-E1 cells. APPL1 siRNA or scrambled siRNA was transfected into MC3T3-E1 cells using the Lipofectamine® 2000 reagent (Invitrogen, Carlsbad, CA, USA), according to the precise protocol provided by the manufacturer. After 6 h of incubation, the medium was replaced with normal growth medium. Following an 18 h culture in normal growth medium, siRNA-transfected cells were lysed and the efficiency of siRNA-mediated APPL1 knockdown was evaluated by western blot.

### Western blotting analysis

Whole protein lysates were prepared using RIPA lysis buffer (Santa Cruz Biotechnology Inc.). SDS-PAGE and western blot analyses were performed using NuPAGE® 4–12% Bis–Tris gradient gels and 0.45 μm Invitrogen polyvinylidene fluoride (PVDF) membranes (Life Technologies, South San Francisco CA, USA). Antibodies were obtained for APPL1 (1 : 2000, Cat. 3858, Cell Signalling Technology, Beverly, MA, USA), PI3 Kinase p110α (1 : 2000, Cat. 4249, Cell Signalling Technology), and β-actin (1 : 1000, Cat. 130656, Santa Cruz Biotechnology), respectively. Secondary antibodies were goat anti-rabbit IgG conjugated to IRDye® 800CW (Cat. 926-32211, LI-COR®, Lincoln, NE, USA). Blotted proteins were detected and quantified using an Odyssey infrared imaging system (LI-COR®, Lincoln, NE, USA).

### Statistical analysis

The results are presented as mean ± SD as calculated from three independent experiments. Statistical significance was evaluated using a one-way analysis of variance (ANOVA) or an independent-sample *t*-test. Data were analyzed using the Student's *t*-test for independent samples. All statistical analyses were performed using SPSS statistical analysis software, Version 17.0. Values of $P < 0.05$ were considered statistically significant.

## Results

### Characterization of chitosan microspheres and PLGA/β-TCP/CM scaffolds

Fig. 1a and b demonstrate the surface morphology of CMs containing APN. The average diameter was 18.59 ± 15.20 μm (Fig. 1a).

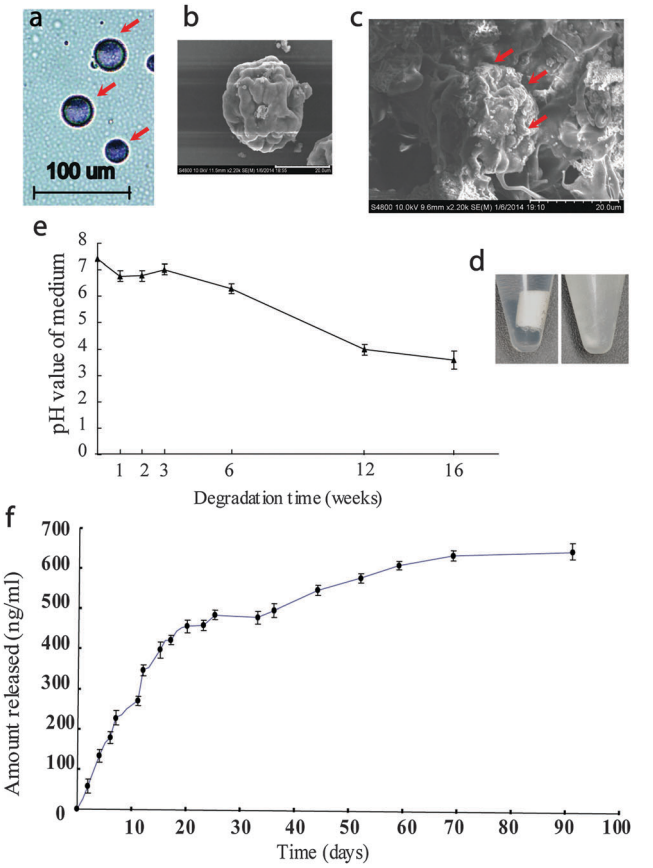


Fig. 1 (a) Optical microscopy image (scale bars = 100 μm) and SEM (b) image (scale bars = 40 μm) of CMs with APN. (c) SEM image of the PLGA/β-TCP scaffold (scale bars = 100 μm) prepared in the presence of CM-APN. Arrows show the CMs (red) in the scaffold. Samples were sputter coated with 50 nm gold particles under vacuum. (d) Appearance of the PLGA scaffold changing from block mass to turbid liquid after 4 months of shaking in PBS solution at 37 °C at a speed of 100 rpm. (e) pH of PLGA/β-TCP scaffold degradation medium after PBS incubation at various time points. (f) *In vitro* release of APN from a PLGA/β-TCP/CM scaffold in PBS solution.

Microspheres presented as spherical, wrinkled structures with a rough and uniform surface (Fig. 1b). SEM images showed that CMs were distributed across the PLGA/β-TCP matrix (Fig. 1c). After 4 months of shaking in PBS solution (0.1 M, pH 7.4) at 37 °C at a speed of 100 rpm, the appearance of the PLGA scaffolds changed from block mass (cylinders with a diameter of 7 mm and a height of 5 mm) to turbid liquid (Fig. 1d). During PBS incubation, the PLGA scaffold pH decreased slowly from weeks 3–6 and then dropped off sharply (from 6.29 to 3.58) from weeks 6–16 (Fig. 1e).

### *In vitro* release kinetics of APN

Fig. 1f shows that after an initial burst at week 1, the release of APN from the scaffold *via* CM was sustained in a linear manner for the first 4 weeks, followed by a slower, more stable manner from week 5 onwards. Consequently, the final amount of APN released from the scaffolds was 68.94% over the entire 91 days.

### Local delivery of APN from biodegradable scaffolds promotes bone formation in APN-KO mice

T-BMD values of μCT were significantly higher in the APN-loaded scaffold group than in the control group (Fig. 2a and b). Moreover, calcein-labeled samples from the APN-loaded scaffold group showed a pattern of continual bone deposition as compared to controls (Fig. 2c). IHC showed that the number of osteoblasts expressing OPN was significantly increased in the APN-loaded scaffold group as compared to the control group (Fig. 3a). APN-loaded scaffold promoting osteogenic activity was further confirmed by OPN and osteocalcin (OCN) expression at the mRNA level (Fig. 3b and c).

### Immunogenic response

As shown in Fig. 4, differences in immunogenic responses between the APN-loaded scaffold and control groups were not significant at 1 week ($P > 0.05$). The percentage of CD4+ T lymphocytes was evaluated in the APN-loaded scaffold group (27.4 ± 4.3%) and in the sham group (26.2 ± 3.7%). The percentage of CD8+ T lymphocytes was also evaluated in the APN-loaded scaffold (14.7 ± 3.1%) and in the sham group (14.9 ± 3.3%). The ratio of CD4+/CD8+ T cells was not significantly different between the two groups.

### gAPN promotes preosteoblast cellular proliferation

The proliferation of preosteoblast MC3T3-E1 cells significantly increased in the APN-treated group as compared to the control group at 24 h ($P = 0.003$) and 48 h ($P = 0.002$) (Fig. 5). Cell growth eventually decreased after 48 h in the APN-treated group.

### APPL1 requires gAPN to induce PI3K and promote MC3T3-E1 proliferation *in vitro*

We found that expression levels of APPL1 (Fig. 6a and b) and PI3K (Fig. 6a and c) increased after 15 and 30 min of gAPN treatments and then decreased at 60 and 120 min as compared to untreated controls, indicating that gAPN treatment activates the PI3K signaling pathway.

To further evaluate whether gAPN activates MC3T3-E1 cell PI3K signaling *via* APPL1, MC3T3-E1 cells were treated with APPL1 siRNA. We found that downregulation of APPL1 expression decreases PI3K expression (Fig. 7).

## Discussion

APN has been found to play an important role in bone metabolism by previous studies, however, observations have been controversial. In this study, we focused on exploring the long-term effects of gAPN on bone metabolism in APN knockout (APN-KO) mice and exploring possible molecular mechanisms underlying APN promotion of osteogenic effects. Microspheres loaded with gAPN presented as spherical, wrinkled structures with a rough and uniform surface (Fig. 1a–c), in line with previous studies that have shown that faster removal of the solvent may lead to a more wrinkled and shrunken profile.[34] This deformation and diminishment could also be induced by preparation of the samples for SEM observations. As a biodegradable material, PLGA has long been in use in surgical

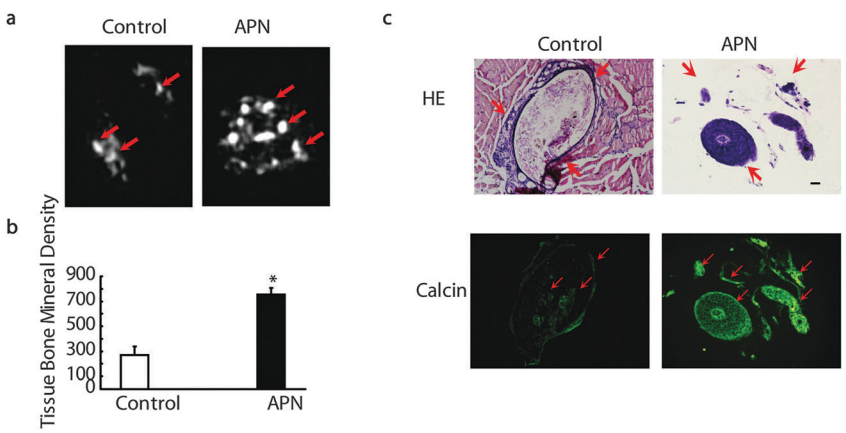


Fig. 2 Local PLGA/β-TCP/CMs with APN transplantation increase bone formation and mineralization in APN-knockout (APN-KO) mice. (a) μCT images of the composite region in APN-KO mice 28 days post-transplantation ($n = 5$). (b) Changes in tissue bone mineral density (T-BMD). Values are mean ± SD for $n = 5$ mice/group. *$P < 0.05$ as determined by the independent-sample $t$-test. (c) H&E and calcein stained sections of the composite transplantation region (indicated by arrow). Scale bar = 20 μm. The full-length H&E picture of the scaffold loaded with APN was included as key data in ESI,† Data 1.

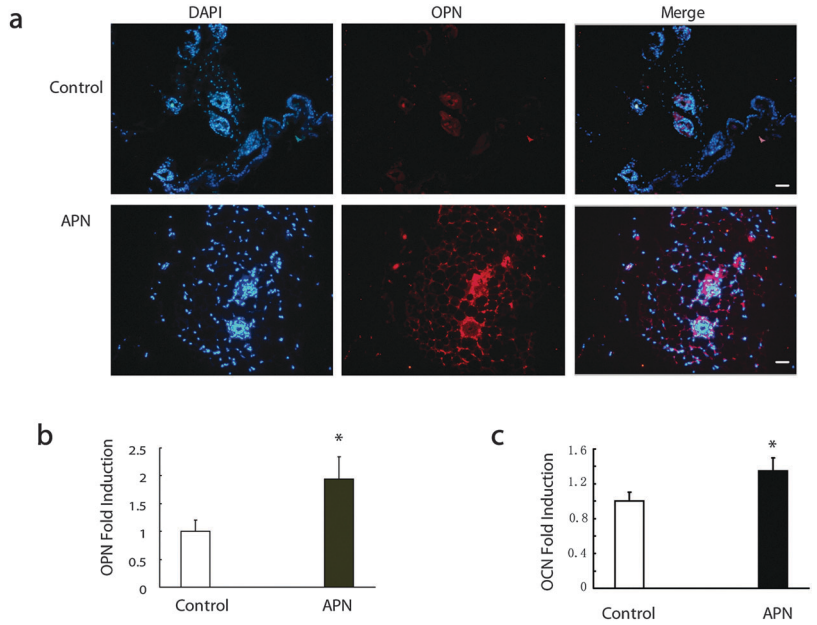


Fig. 3 Osteogenic marker expression is enhanced following transplantation with PLGA/β-TCP/CMs containing APN in APN-KO mice for 28 days. IHC analysis of nuclear (blue), OPN (red), and merged images in transplantation sections (a). Scale bars = 20 μm. The APN-loaded scaffold promoting osteogenic activity was further confirmed by OPN and osteocalcin (OCN) expression at the mRNA level (b and c).

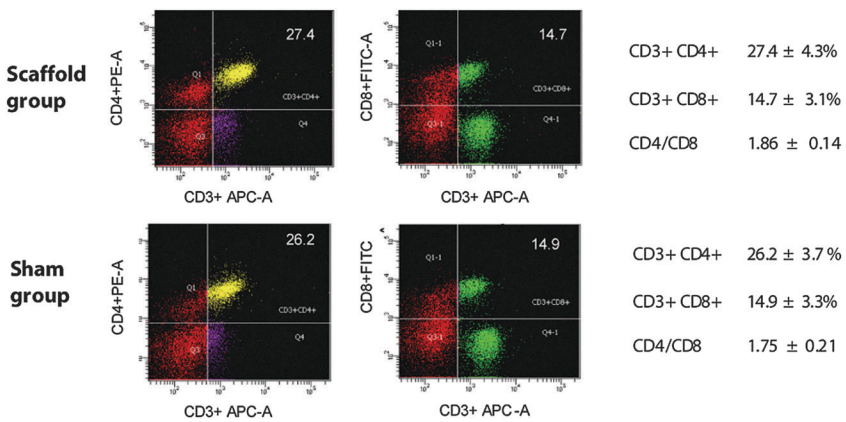


Fig. 4 Differences in immunogenic responses between the APN-loaded scaffold and sham controls were not significant ($P > 0.05$). The percentage of CD4+ T lymphocytes in APN-loaded scaffold groups averaged 27.4 ± 4.3% and in sham groups, 26.2 ± 3.7%. The percentage of CD8+ T lymphocytes of APN loaded scaffold groups averaged 14.7 ± 3.1% and in sham groups, 14.9 ± 3.3%. The ratios of CD4+/CD8+ T cells were not significantly different between the two groups ($P > 0.05$).

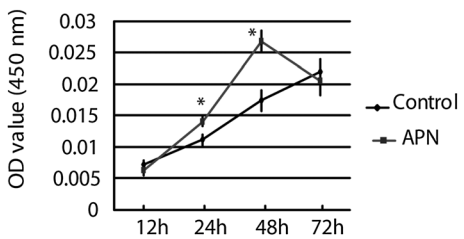


Fig. 5 Cell proliferation analysis. gAPN promotes preosteoblast (MC3T3-E1) cellular proliferation at 24 h ($P = 0.003$) and 48 h ($P = 0.002$). *$P < 0.05$ by one-way ANOVA.

applications with bone regenerative materials.[4] However, these delivery systems have unpredictable release rates, often displaying a high initial burst.[4,35,36] Luginbuehl *et al.* reported that the PLGA scaffold should be used solely for protein-controlled delivery[36] as PLGA/β-TCP scaffolds loaded with tetracycline produced an initial burst of about 30% of the total dose within 12 h, followed by rapid release of 90% of the remaining drug within 4 days. Furthermore, the use of organic solvents to load APN into the polymer scaffold may cause structural damage to growth factor proteins, reducing their bioactivity. Therefore, CMs were introduced into a PLGA/β-TCP scaffold to produce a sustained delivery rate of biologically active cytokines over an extended period of time. In our study, CMs were embedded into

 

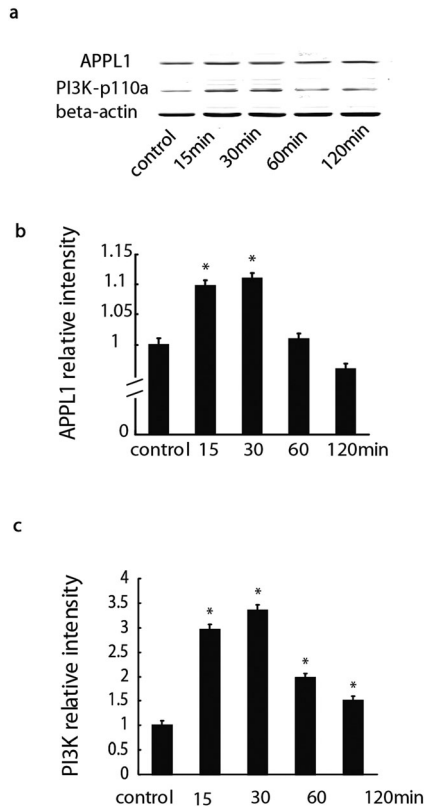


Fig. 6 APN treatment can promote MC3T3-E1 cell proliferation. (a) APPL1 and PI3K expression in MC3T3-E1 cells was enhanced following 0.1 nM gAPN treatment. (b and c) Relative intensities of APPL1 (b) and PI3K (c). *$P < 0.05$ by one-way ANOVA. Cropped blots were used in the main figures and all gels were run under the same experimental conditions. Full-length blots are included as key data in ESI,† Data 2.

PLGA/β-TCP scaffolds (Fig. 1a–d). CMs loaded with gAPN were developed by emulsion-ionic cross-linking in the presence of TPP to prevent negative chemical crosslinking effects in a protein/peptide context.

Besides the need for a controlled drug delivery system, optimized degradation rates and resorption of the bone substitute are other important aspects for a material to be widely used for guided bone regeneration. There was no significant change in the pH value for the initial 4 weeks, because dissolution of the chitosan component and β-TCP was able to alkalize the medium. Over the subsequent 10 weeks, pH dropped sharply from 6.29 to 3.58 (Fig. 1e). Therefore, the median pH value depends upon both the degradation rate of the PLGA matrix and the dissolution profiles of the CMs and β-TCP. This result was in agreement with previous studies.[37,38] *In vitro* degradation therefore revealed that gAPN-CM-loaded scaffolds have an advantage over other bone repair applications, as β-TCP-stimulated natural bone structure formation and alkaline dissolution of CMs and β-TCP are able to counteract the effects of the degraded acidic molecules of PLGA on pH; this reduced overall PLGA degradation.

Release of gAPN from CM-loaded scaffolds gradually increased for the first 24 days, followed by a slow and stable release up to day 91 (Fig. 1f). Because of the short clearance time of gAPN in mice (32.4–83.3 min)[39] and the rapid loss of APN bioactivity when administered in solution *in vivo*, a controlled release system was designed for loading. Our microsphere–scaffold delivery composite improved the function of APN by maintaining local cytokine concentrations at ideal levels for longer periods of time in accordance with continuous and sustained release. As previous studies have indicated conflicting functions for gAPN in bone metabolism,[30,40] we explored the effects of long-term delivery of gAPN on bone regeneration *in vivo*. We used an APN-KO mouse model to study and evaluate the critical role of gAPN in bone physiology. μCT data showed that local, long-term gAPN delivery confers greater T-BMD in APN-KO mice than that found in control mice 4 weeks post-implantation (Fig. 2a and b). Histological analysis further confirmed that long-term APN treatment increases bone formation and mineralization (Fig. 2c). Additionally, at 4 weeks post-implantation, we found that the scaffold material was well combined with the surrounding muscle tissue, indicating little to no inflammatory reaction to the hydrolytic degradation of PLGA (Fig. 2c). These results are consistent with those showing significantly retarded growth of bone explants in APN-KO mice;[41] in addition, AdipoR1 mice had higher bone volumes and trabecular numbers than wild-type mice.[42] We thereby evaluated the number of osteoblasts per bone surface and found that there were significantly more in the APN-loaded group as compared to the control group (Fig. 3), which is concordant with data showing AdipoR1 mice with higher bone formation marker expression levels than wild-type mice.[42]

Due to its excellent biocompatibility and biodegradability, PLGA is one of the most widely used biodegradable synthetic biomaterials. However, PLGA is composed of the random polymerization of two monomers (lactic acid and glycolic acid) and the hydrolytic or enzymatic degradation of PLGA results in relatively acidic byproducts that can induce acute or chronic inflammatory responses.[2] To analyze acute inflammatory responses, the percentages of CD4+ and CD8+ lymphocyte subpopulations and the ratios of CD4+/CD8+ T lymphocytes in peripheral blood from APN-KO mice with either gAPN-loaded or control scaffolds were detected by flow cytometry (Fig. 4). This testing index reflects certain acute immunogenic response patterns, such as those found in graft-versus-host disease (GVHD)[43] and transplant rejection.[44] In the present study, no significant differences in acute immunogenic responses were found between the gAPN-loaded scaffold and blank control groups through week 1 post-implantation ($P > 0.05$) (Fig. 4). This indicates an acceptable biocompatibility for local PLGA/β-TCP/CM scaffolds.

To further explore the bioactivity of gAPN released from PLGA/β-TCP/CM scaffolds and the role of gAPN in the bone formation process, we studied the proliferation effects of treatment with gAPN extracted from PLGA/β-TCP/CM scaffolds or APPL1 siRNA on the MC3T3-E1 (preosteoblasts) cell line. In the MC3T3-E1 cell proliferation experiment, we demonstrated that gAPN extracted from PLGA/β-TCP/CM scaffolds promotes cell proliferation following 24 h and 48 h of culture, respectively (Fig. 5). In the APN-treated group, cell growth decreased after 48 h.

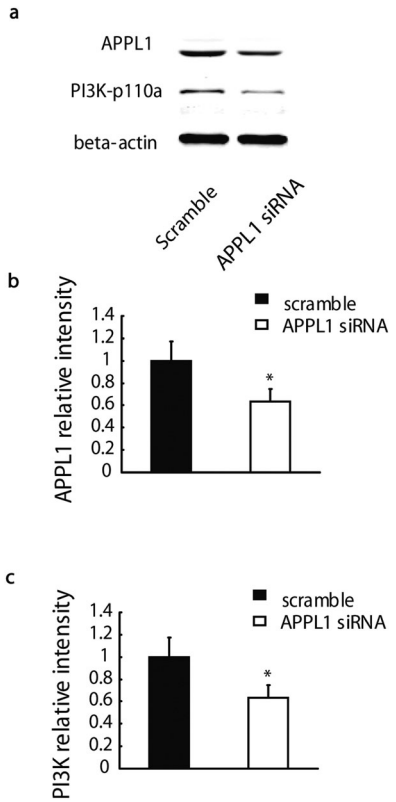


Fig. 7 siRNA-mediated knockdown of APPL1 in MC3T3-E1 cells and gAPN treatment. (a) APPL1 siRNA pre-treatment down-regulated PI3K expression in MC3T3-E1 cells. (b and c) Relative intensities of APPL1 (b) and PI3K (c). *$P < 0.05$ by the independent-sample $t$-test. Cropped blots were used in the main figures and all gels were run under the same experimental conditions. Full-length blots are included as key data in ESI,† Data 2.

The assay was performed following 7 days of extraction in MEM culture medium; 7 days would appear to correspond to a release of quite a small amount of gAPN. As such, a longer duration extraction process may have resulted in the extraction of more APN molecules from the scaffolds. Moreover, gAPN treatment increased APPL1 and PI3K expression in a time-dependent manner within the first 30 min (Fig. 6), suggesting a potential role of APPL1 and PI3K in osteoblast cell proliferation. Indeed, the western blot results also point to an enhancement of cell proliferation by gAPN over a short period of time (48 h). Furthermore, considering that PI3K plays a central role in osteoblast proliferation and differentiation,[45,46] we were able to show that knockdown of APPL1 expression decreases PI3K expression in MC3T3-E1 cells (Fig. 7). Taken together, these data provide partial insight into the role of the APPL1/PI3K signaling pathway in regulating osteoblast proliferation and differentiation in response to gAPN treatment. These results are in agreement with previous studies that showed that gAPN induces osteoblastogenesis and suppresses osteoclastogenesis, enhancing bone formation.[23,41,42,47–49] While Luo *et al.* showed that gAPN inhibits osteoprotegerin expression in human osteoblasts,[50] this controversial observation may have been caused by LPS contamination, which could have created confusion as to the true function of gAPN. In our study, we avoided a potential confounding endotoxin effect by processing gAPN using an endotoxin removal process followed by desalting. Another possible reason is that our controlled release of gAPN delivery could increase the duration of gAPN, enhancing its effects.

In summary, our data demonstrate that a PLGA/B-TCP/CM scaffold delivery system can provide sustained gAPN release for 91 days. Extended gAPN delivery by composite scaffolds resulted in extensive bone formation in male APN-KO mice, indicating that a sustained and controlled delivery of gAPN increases the bone regenerative efficacy of the PLGA and β-TCP composite. The local, sustained delivery system for gAPN developed in this study could provide a powerful new modality for bone regeneration.

## Disclosures

No conflicts of interest, financial or otherwise, are declared by any of the authors.

## Acknowledgements

We thank Jie Du and Li-Xin Jia at the Beijing AnZhen Hospital, Capital Medical University, and Peoples Republic of China for providing APN knockout mice. We want to thank Dana Murray for her secretarial assistance in the preparation of this manuscript. This work was supported by the National Natural Science Foundation of China, grant number 81300851, which was awarded to Yu-wei Wu, and the Beijing Municipal Natural Science Foundation, Grants numbers SKLODd2009001 and Z15110400370000, which were awarded to Zhi-hui Tang.

## References

1 J. Henkel, M. A. Woodruff, D. R. Epari, R. Steck, V. Glatt, I. C. Dickinson, P. F. Choong, M. A. Schuetz and D. W. Hutmacher, *Bone Res.*, 2013, **1**, 216–248.
2 J. Liao, K. Shi, Q. Ding, Y. Qu, F. Luo and Z. Qian, *J. Biomed. Nanotechnol.*, 2014, **10**, 3085–3104.
3 S. Fu, P. Ni, B. Wang, B. Chu, J. Peng, L. Zheng, X. Zhao, F. Luo, Y. Wei and Z. Qian, *Biomaterials*, 2012, **33**, 8363–8371.
4 L. Wang, L. Zheng, C. Li, S. Dong, L. A and Y. Zhou, *Biomed. Eng. Online*, 2013, **12**, 99.
5 S. E. Petricca, K. G. Marra and P. N. Kumta, *Acta Biomater.*, 2006, **2**, 277–286.
6 S. Liao, F. Watari, Y. Zhu, M. Uo, T. Akasaka, W. Wang, G. Xu and F. Cui, *Dent. Mater.*, 2007, **23**, 1120–1128.
7 R. Nakajima, M. Ono, E. S. Hara, Y. Oida, S. Shinkawa, H. T. Pham, K. Akiyama, W. Sonoyama, K. Maekawa and T. Kuboki, *J. Dent. Res.*, 2014, **93**, 1133–1140.
8 F. Nudelman, K. Pieterse, A. George, P. H. Bomans, H. Friedrich, L. J. Brylka, P. A. Hilbers, G. de With and N. A. Sommerdijk, *Nat. Mater.*, 2010, **9**, 1004–1009.
9 J. Varshosaz, *Expert Opin. Drug Delivery*, 2007, **4**, 263–273.

 

10 F. Pati, T. H. Song, G. Rijal, J. Jang, S. W. Kim and D. W. Cho, *Biomaterials*, 2015, **37**, 230–241.
11 J. Kulkova, N. Moritz, E. O. Suokas, N. Strandberg, K. A. Leino, T. T. Laitio and H. T. Aro, *J. Mech. Behav. Biomed. Mater.*, 2014, **40**, 190–200.
12 Y. B. Kim and G. Kim, *Appl. Phys. A: Mater. Sci. Process.*, 2012, **108**, 949–959.
13 M. R. Urist, A. Lietze and E. Dawson, *Clin. Orthop. Relat. Res.*, 1984, 277–280.
14 A. M. Barradas, H. A. Fernandes, N. Groen, Y. C. Chai, J. Schrooten, J. van de Peppel, J. P. van Leeuwen, C. A. van Blitterswijk and J. de Boer, *Biomaterials*, 2012, **33**, 3205–3215.
15 P. Hanseler, M. Ehrbar, A. Kruse, E. Fischer, R. Schibli, C. Ghayor and F. E. Weber, *J. Biomed. Mater. Res., Part A*, 2015, **103**, 628–638.
16 Y. Kang, S. Kim, J. Bishop, A. Khademhosseini and Y. Yang, *Biomaterials*, 2012, **33**, 6998–7007.
17 Y. Kang, S. Kim, A. Khademhosseini and Y. Yang, *Biomaterials*, 2011, **32**, 6119–6130.
18 S. Bitencourt Cda, L. B. Silva, P. A. Pereira, G. M. Gelfuso and L. H. Faccioli, *Colloids Surf., B*, 2015, **136**, 678–686.
19 C. K. Wang, M. L. Ho, G. J. Wang, J. K. Chang, C. H. Chen, Y. C. Fu and H. H. Fu, *Biomaterials*, 2009, **30**, 4178–4186.
20 R. Tuli, S. Tuli, S. Nandi, X. Huang, P. A. Manner, W. J. Hozack, K. G. Danielson, D. J. Hall and R. S. Tuan, *J. Biol. Chem.*, 2003, **278**, 41227–41236.
21 T. Takahashi, T. Ogasawara, J. Kishimoto, G. Liu, H. Asato, T. Nakatsuka, E. Uchinuma, K. Nakamura, H. Kawaguchi, U. I. Chung, T. Takato and K. Hoshi, *Cell Transplant*, 2005, **14**, 683–693.
22 H. Pareja-Galeano, A. Santos-Lozano, F. Sanchis-Gomar, C. Fiuza-Luces, N. Garatachea, B. G. Galvez, A. Lucia and E. Emanuele, *Mech. Ageing Dev.*, 2016, DOI: 10.1016/j.mad.2016.02.014.
23 Y. Wu, Q. Tu, P. Valverde, J. Zhang, D. Murray, L. Q. Dong, J. Cheng, H. Jiang, M. Rios, E. Morgan, Z. Tang and J. Chen, *Am. J. Physiol.: Endocrinol. Metab.*, 2014, **306**, E1418–E1430.
24 T. Yamauchi, J. Kamon, H. Waki, Y. Terauchi, N. Kubota, K. Hara, Y. Mori, T. Ide, K. Murakami, N. Tsuboyama-Kasaoka, O. Ezaki, Y. Akanuma, O. Gavrilova, C. Vinson, M. L. Reitman, H. Kagechika, K. Shudo, M. Yoda, Y. Nakano, K. Tobe, R. Nagai, S. Kimura, M. Tomita, P. Froguel and T. Kadowaki, *Nat. Med.*, 2001, **7**, 941–946.
25 T. S. Tsao, H. F. Lodish and J. Fruebis, *Eur. J. Pharmacol.*, 2002, **440**, 213–221.
26 U. B. Pajvani, X. Du, T. P. Combs, A. H. Berg, M. W. Rajala, T. Schulthess, J. Engel, M. Brownlee and P. E. Scherer, *J. Biol. Chem.*, 2003, **278**, 9073–9085.
27 H. Waki, T. Yamauchi, J. Kamon, Y. Ito, S. Uchida, S. Kita, K. Hara, Y. Hada, F. Vasseur, P. Froguel, S. Kimura, R. Nagai and T. Kadowaki, *J. Biol. Chem.*, 2003, **278**, 40352–40363.
28 I. Padmalayam and M. Suto, *Curr. Pharm. Des.*, 2013, **19**, 5755–5763.
29 T. Villarreal-Molina, C. Posadas-Romero, S. Romero-Hidalgo, E. Antunez-Arguelles, A. Bautista-Grande, G. Vargas-Alarcon, E. Kimura-Hayama, S. Canizales-Quinteros, J. G. Juarez-Rojas, R. Posadas-Sanchez, G. Cardoso-Saldana, A. Medina-Urrutia, C. Gonzalez-Salazar Mdel, R. Martinez-Alvarado, E. Jorge-Galarza and A. Carnevale, *PLoS One*, 2012, **7**, e49285.
30 P. M. van der Kraan, P. Buma, T. van Kuppevelt and W. B. van den Berg, *Osteoarthritis Cartilage*, 2002, **10**, 631–637.
31 I. Kanazawa, T. Yamaguchi and T. Sugimoto, *Metabolism*, 2010, **59**, 1252–1256.
32 M. C. Zillikens, A. G. Uitterlinden, J. P. van Leeuwen, A. L. Berends, P. Henneman, K. W. van Dijk, B. A. Oostra, C. M. van Duijn, H. A. Pols and F. Rivadeneira, *Calcif. Tissue Int.*, 2010, **86**, 116–125.
33 M. L. Bouxsein, S. K. Boyd, B. A. Christiansen, R. E. Guldberg, K. J. Jepsen and R. Muller, *J. Bone Miner. Res.*, 2010, **25**, 1468–1486.
34 A. A. Zaghloul, *Pharmazie*, 2006, **61**, 775–779.
35 F. J. Verstraete, *J. S. Afr. Vet. Assoc.*, 1983, **54**, 231–238.
36 V. Luginbuehl, K. Ruffieux, C. Hess, D. Reichardt, B. von Rechenberg and K. Nuss, *J. Biomed. Mater. Res., Part B*, 2010, **92**, 341–352.
37 X. Niu, Y. Luo, Y. Li, C. Fu, J. Chen and Y. Wang, *J. Biomed. Mater. Res., Part A*, 2008, **84**, 908–916.
38 M. Chen, S. Gao, M. Dong, J. Song, C. Yang, K. A. Howard, J. Kjems and F. Besenbacher, *ACS Nano*, 2012, **6**, 4835–4844.
39 N. Halberg, T. D. Schraw, Z. V. Wang, J. Y. Kim, J. Yi, M. P. Hamilton, K. Luby-Phelps and P. E. Scherer, *Diabetes*, 2009, **58**, 1961–1970.
40 K. Oshima, A. Nampei, M. Matsuda, M. Iwaki, A. Fukuhara, J. Hashimoto, H. Yoshikawa and I. Shimomura, *Biochem. Biophys. Res. Commun.*, 2005, **331**, 520–526.
41 Q. Tu, J. Zhang, L. Q. Dong, E. Saunders, E. Luo, J. Tang and J. Chen, *J. Biol. Chem.*, 2011, **286**, 12542–12553.
42 Y. Y. Lin, C. Y. Chen, T. Y. Chuang, Y. Lin, H. Y. Liu, H. J. Mersmann, S. C. Wu and S. T. Ding, *Bone*, 2014, **64**, 147–154.
43 J. W. Gratama, A. Naipal, P. Oljans, F. E. Zwaan, L. F. Verdonck, T. de Witte, J. M. Vossen, R. L. Bolhuis, G. C. de Gast and J. Jansen, *Blood*, 1984, **63**, 1416–1423.
44 G. A. Bishop, B. M. Hall, G. G. Duggin, J. S. Horvath, A. G. Sheil and D. J. Tiller, *Kidney Int.*, 1986, **29**, 708–717.
45 Y. X. Gu, J. Du, M. S. Si, J. J. Mo, S. C. Qiao and H. C. Lai, *J. Biomed. Mater. Res., Part A*, 2013, **101**, 748–754.
46 A. R. Guntur and C. J. Rosen, *J. Endocrinol.*, 2011, **211**, 123–130.
47 Y. Pu, H. Wu, S. Lu, H. Hu, D. Li, Y. Wu and Z. Tang, *J. Dent. Res.*, 2016, DOI: 10.1177/0022034516636853.
48 T. Chen, Y. W. Wu, H. Lu, Y. Guo and Z. H. Tang, *Biochem. Biophys. Res. Commun.*, 2015, **461**, 237–242.
49 H. Hu, Y. Pu, S. Lu, K. Zhang, Y. Guo, H. Lu, D. Li, X. Li, Z. Li, Y. Wu and Z. Tang, *Int. J. Mol. Sci.*, 2015, **16**, 24946–24964.
50 X. H. Luo, L. J. Guo, H. Xie, L. Q. Yuan, X. P. Wu, H. D. Zhou and E. Y. Liao, *J. Bone Miner. Res.*, 2006, **21**, 1648–1656.